height in the sequence. Over this same interval, the rims of the grains are more sodic than the cores (Figure 6.C). No lithological control over the An content is noted.

Plagioclase separates range from a minimum value of An_{54}, to a maximum of An_{84}. The overall trend is one where the An content decreases with an increase height up through the stratigraphic succession. The sample at -338m is unusually high, with an An content of 81. This is followed by a profile, which is relatively constant to -140m, about the value An_{71-75}. Two exceptions are found at -236m and -195m, where the respective An contents of 84 and 66 are found. These may be a result of alteration. At -134m and above, values decrease up to 45m, where an An of 54 is found. Upward from this point, there is a reversal in the trend to the 111m sample, which has an anorthite content of 69 before a slight drop to An_{66} at 136m, the top of the sampled section.

Wt % K_2O

Average core values range from 0.14 - 0.23 wt % and are more constrained than the average rim values, which have a minimum of 0.10 and a maximum of 0.28 wt %. Potassium enrichment is found to alternate from cores to rims throughout the succession. The profile in Figure 6.C shows that the trend is relatively constant for the entire sampled section. It indicates a very gradual increase in the potassium concentration, from the Critical Zone up through the Main Zone, particularly in the cores. More noticeably, between -159m and -140m the potassium concentration decreases from 0.20 to 0.14 wt %, which coincides with the lithology changing from a mottled anorthosite to gabbronorite. An increase to 0.19 wt % occurs at -115m, where another mottled anorthosite is encountered. The remaining samples contain values varying between 0.15 and 0.23 wt %, and do not appear to follow this trend, making lithological control unlikely.

Minimum and maximum values for the plagioclase separates are 0.05 and 1.35 wt % K_2O. For the majority of the Main Zone, and the few samples taken from the Critical Zone, the profile is one which varies between 0 - 0.5 wt %. From -92m upwards however, the potassium profile indicates an increase in value to the top of the Main Zone, with the sample at -9m indicating a maximum of 1.35 wt % K_2O. This sample is not plotted in Figure 6.C as it would distort the profile for the remainder of the samples. This variation between the two data sets is explained by the fact that the microprobe analyses was taken from pristine plagioclase grains, whereas the XRF analyses of the plagioclase separates may have incorporated some K-rich feldspar which would increase the overall wt % K_2O concentration. The samples that are taken from the Upper Zone indicate a return to a similar trend to that of the Main Zone, varying between 0 - 0.5 wt % K_2O.

Wt % FeO

Core values fall between 0.08 - 0.14 wt % and rim averages span 0.10 - 0.24 wt %. The profiles for both are relatively constant throughout the Critical and Main Zones, with little variation (Figure 6.C). There is no apparent lithological control over this element.

Plagioclase separates have minimum and maximum values of 0.08 and 2.11 wt % FeO, respectively. For the majority of the section they are contained within the range of 0 - 0.5 wt % FeO. Within the anorthosites of the Merensky and Bastard Cyclic Units, the wt % FeO concentration increases to 0.83 wt % FeO. This drops back down to an average of 0.40 wt % within the gabbronorite of the Main Zone. A further increase in FeO concentration occurs directly below the boundary between the Main and Upper Zones. From -36m to -19m, the FeO concentration increases from 0.24 to 1.30 wt %, which marks the beginning of more widely fluctuating values that continue into the Upper Zone. The Upper Zone values range from 0.47 - 2.11 wt % FeO, and indicate a general upwards increase, which may be ascribed to small inclusions of magnetite enclosed within the plagioclase, although no particular trend is defined.

6.1.1.4: D1 Summary

Many of the significant differences in the concentration of the major and minor elements in the minerals described above, occur across the interval between -159m and -140m. Both the clinopyroxene and the orthopyroxene in the Main Zone vary similarly, although the average clinopyroxene cores are richer in magnesian, titanium, aluminium and chromium than the orthopyroxenes at the corresponding depths.

Magnesium is found in the greatest amounts in the cores of the clinopyroxene and orthopyroxenes within the more mafic units, and in the lowest quantities in the anorthosites. Although both pyroxenes indicate a similar trend, orthopyroxene contain less magnesium than clinopyroxene for both cores and rims, which differ by approximately 10% and 12%, respectively.

Titanium concentration does not appear to vary throughout the succession, as there is a wide spread of data, which obscures any systematic trends, nor does it appear to be controlled by lithology. The aluminium concentration varies slightly throughout the succession, but does not appear to be controlled by the lithology. Larger amounts occur in the cores and rims of the clinopyroxenes than in the corresponding orthopyroxene grains.

Lithological control is apparent only for pyroxene cores. Within anorthosites, clinopyroxene cores are enriched with chromium, but in more mafic units they are depleted. The opposite is true for the

orthopyroxene cores within the same anorthositic and mafic units. Overall, orthopyroxene contains less chromium, but shows little variation throughout the sampled section. However, the chromium concentration within the clinopyroxenes decreases upwards.

The composition of plagioclase grains, with respect to the major and minor elements, is not dictated by the lithology, as both minimum and maximum values occur within both anorthosites and gabbronorites.

6.1.1.5: Wo-En-Fs Ternary Systems

Core data for clinopyroxene-orthopyroxene pairs are plotted with tie lines on the ternary plot Wo-En-Fs. The isotherms at 0Kbar are calculated for the pyroxene quadrilateral, as in Figure 6.D. These indicate the various isotherms on the clinopyroxene - orthopyroxene solvus (Davidson and Lindsley, 1989) and subsequently the temperatures at which the clinopyroxenes and orthopyroxenes within D1 equilibrated. These temperatures range between 600° and 850° at 0Kbar for the clinopyroxene, and between 900° - 950° at 0Kbar for the orthopyroxene.

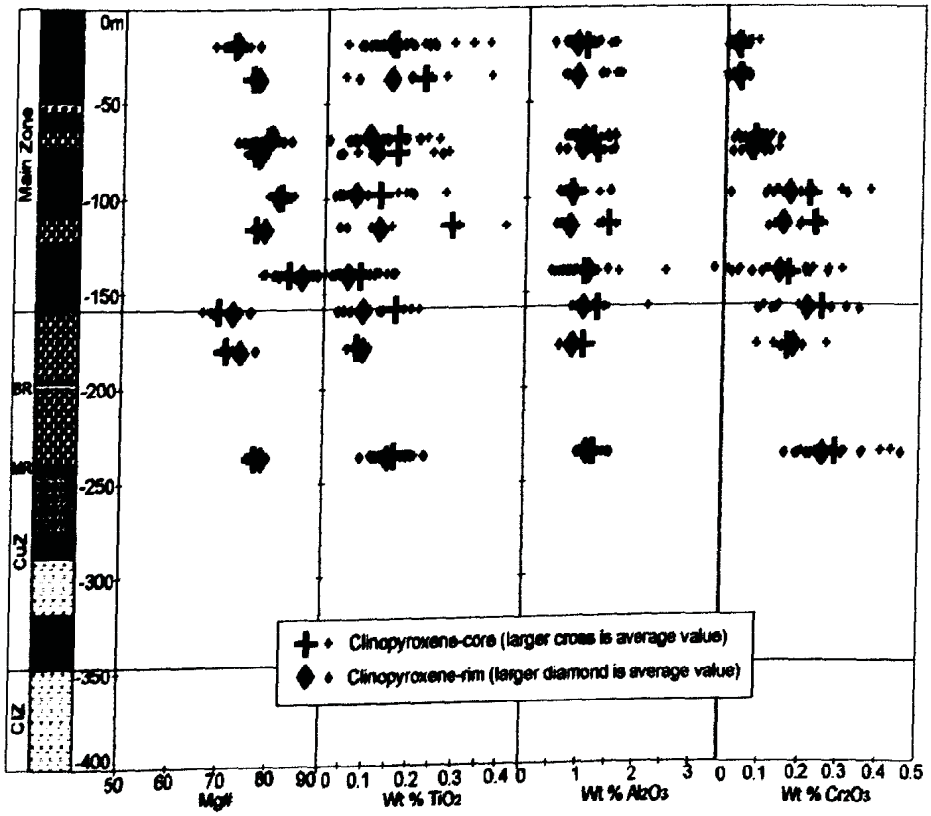

Figure 6.A Electron microprobe analyses of clinopyroxene cores and rims from samples in D1. The Mg content, wt % TiO_2, Al_2O_3 and Cr_2O_3 are plotted against the stratigraphic column and depth relative to the MZ/UZ boundary, which includes the positions of the Merensky Reef (MR) and the Bastard Reef (BR).

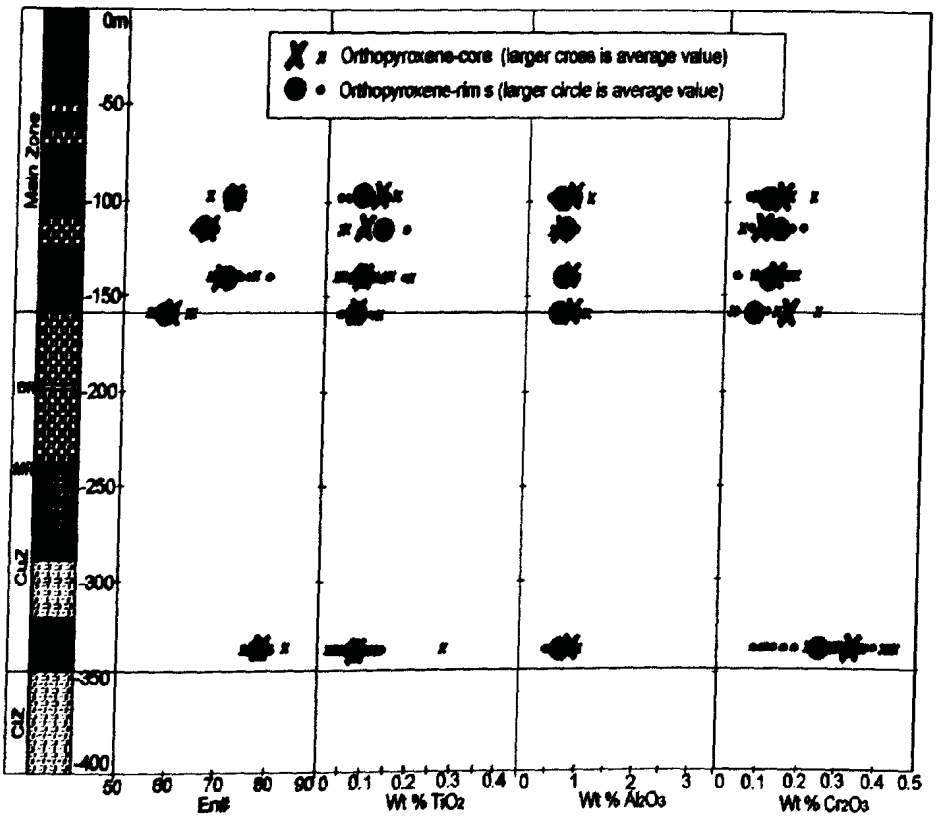

Figure 6.B Electron microprobe analyses of orthopyroxene cores and rims from samples in D1. The En content, wt % TiO_2, Al_2O_3 and Cr_2O_3 are plotted against the stratigraphic column and depth relative to the MZ/UZ boundary, which includes the positions of the Merensky Reef (MR) and the Bastard Reef (BR).

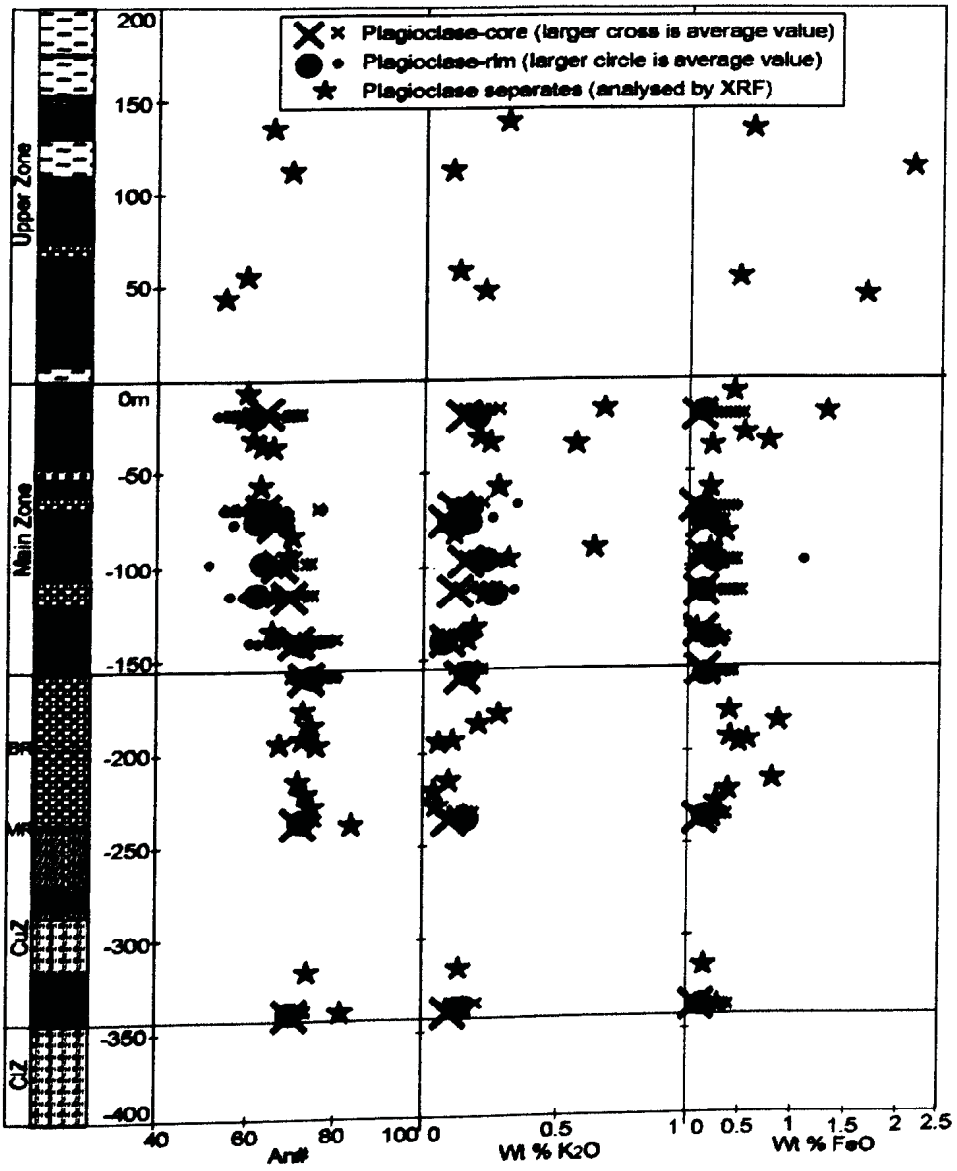

Figure 6.C Electron microprobe analyses of plagioclase cores and rims from samples in D1. The An content, wt % K_2O and FeO are plotted against the stratigraphic column and depth relative to the MZ/UZ boundary, which includes the positions of the Merensky Reef (MR) and the Bastard Reef (BR).

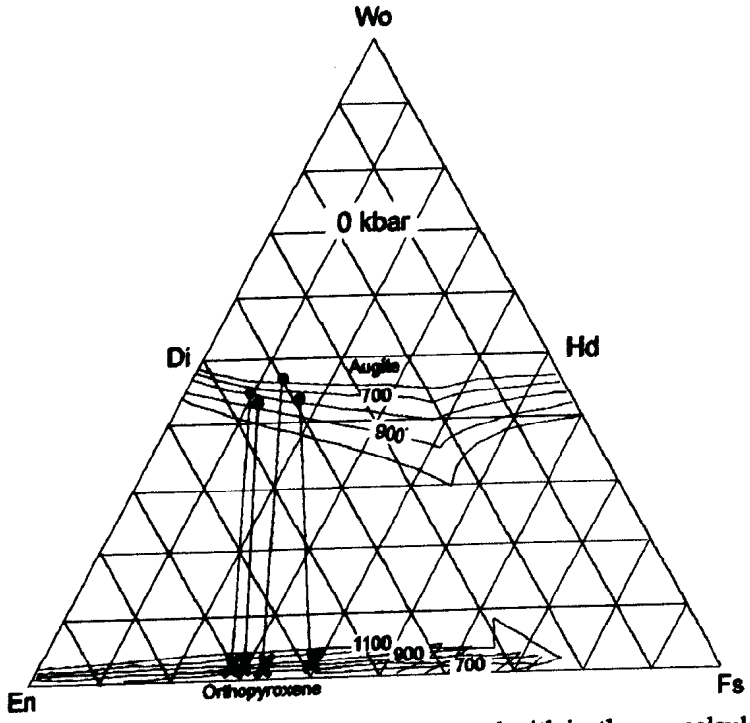

Figure 6.D D1 clinopyroxene and orthopyroxene pairs plotted with isotherms calculated for 0Kbar, after Davidson and Lindlsey (1989).

Table 6.ii Average D1 clinopyroxene values for both core and rim analyses as determined by electron microprobe, with Fe^{3+} calculated from stoichiometry

	Clinopyroxene Cores										Clinopyroxene Rims									
Sample	D1.259	D1.276	D1.309	D1.316	D1.338	D1.355	D1.380	D1.399	D1.419	D1.476	D1.259	D1.276	D1.309	D1.316	D1.338	D1.355	D1.380	D1.399	D1.419	D1.476
Depth*	-19	-36	-69	-76	-96	-115	-140	-159	-179	-236	-19	-36	-69	-76	-96	-115	-140	-159	-179	-236
SiO_2	53.80	55.16	54.10	53.61	54.75	53.80	54.56	53.52	53.85	53.53	54.01	55.96	54.38	53.82	54.96	54.72	54.89	54.13	54.76	53.63
TiO_2	0.20	0.23	0.16	0.16	0.13	0.29	0.10	0.16	0.06	0.18	0.15	0.13	0.10	0.11	0.07	0.12	0.07	0.06	0.09	0.15
Al_2O_3	1.06	1.41	1.26	1.27	0.93	1.46	1.19	1.40	1.01	1.25	0.86	0.88	1.00	0.93	0.79	0.78	1.15	0.96	0.80	1.16
FeO	8.77	8.10	7.15	8.06	6.37	7.45	5.59	9.90	9.33	7.41	8.68	8.32	7.39	8.04	6.07	6.87	4.70	9.45	8.90	7.42
Cr_2O_3	0.04	0.03	0.09	0.11	0.22	0.23	0.16	0.25	0.16	0.29	0.03	0.02	0.07	0.07	0.17	0.15	0.14	0.21	0.18	0.25
MnO	0.26	0.29	0.25	0.33	0.19	0.18	0.13	0.26	0.29	0.20	0.26	0.26	0.26	0.34	0.19	0.20	0.11	0.23	0.30	0.20
MgO	12.87	14.63	14.50	14.93	15.74	13.57	15.76	13.12	13.09	14.16	12.93	14.90	14.92	15.42	15.95	13.86	15.96	13.18	13.58	14.19
CaO	22.25	19.65	21.60	20.82	20.82	22.20	21.87	20.56	19.11	20.90	22.08	19.87	21.08	20.37	20.95	22.63	22.08	20.97	18.67	20.85
Na_2O	0.18	0.20	0.27	0.16	0.30	0.14	0.24	0.22	0.37	0.32	0.15	0.39	0.21	0.35	0.27	0.20	0.26	0.17	0.30	0.23
Total	99.24	99.73	99.40	99.49	99.46	99.33	99.42	99.41	97.31	98.25	99.16	100.77	99.43	99.47	99.45	99.33	99.39	99.39	97.62	98.10
WO	47.41	42.21	45.42	43.23	43.52	47.20	45.09	43.96	42.62	44.90	46.93	42.01	44.09	42.11	43.62	47.99	45.96	44.74	41.72	44.80
EN	37.56	43.72	42.43	43.13	45.78	40.14	45.62	39.05	40.62	42.33	38.24	43.83	43.42	44.36	46.21	40.31	46.22	39.13	42.22	42.42
FS	15.02	14.07	12.15	13.64	10.71	12.67	9.29	16.97	16.75	12.77	14.84	14.16	12.49	13.53	10.18	11.71	7.82	16.13	16.05	12.78
Mg #	71.43	75.65	77.73	75.98	81.04	78.02	83.08	69.71	70.80	76.83	72.05	75.58	77.65	76.63	81.95	77.49	85.53	70.81	72.45	76.84
TSi	2.03	2.06	2.02	2.00	2.03	2.02	2.02	2.02	2.07	2.02	2.04	2.06	2.03	2.00	2.04	2.05	2.03	2.04	2.10	2.03
TAl	0.00	0.00	0.00	0.00	0.00	0.00	0.00	0.00	0.00	0.00	0.00	0.00	0.00	0.00	0.00	0.00	0.00	0.00	0.00	0.00
TFe3	0.00	0.00	0.00	0.00	0.00	0.00	0.00	0.00	0.00	0.00	0.00	0.00	0.00	0.00	0.00	0.00	0.00	0.00	0.00	0.00
M1Al	0.05	0.06	0.06	0.06	0.04	0.07	0.05	0.06	0.05	0.06	0.04	0.04	0.04	0.04	0.03	0.03	0.05	0.04	0.04	0.05
M1Ti	0.01	0.01	0.00	0.00	0.00	0.01	0.00	0.01	0.00	0.01	0.00	0.00	0.00	0.00	0.00	0.00	0.00	0.00	0.00	0.00
M1Fe3	0.00	0.00	0.00	0.00	0.00	0.00	0.00	0.00	0.00	0.00	0.00	0.00	0.00	0.00	0.00	0.00	0.00	0.00	0.00	0.00
M1Fe2	0.23	0.12	0.13	0.11	0.06	0.16	0.07	0.19	0.20	0.13	0.23	0.14	0.12	0.10	0.08	0.20	0.07	0.21	0.18	0.14
M1Cr	0.00	0.00	0.00	0.00	0.01	0.01	0.01	0.01	0.01	0.01	0.00	0.00	0.00	0.00	0.01	0.00	0.00	0.01	0.01	0.01
M1Mg	0.71	0.81	0.81	0.83	0.87	0.76	0.87	0.74	0.75	0.80	0.73	0.82	0.83	0.86	0.88	0.76	0.88	0.74	0.78	0.80
M2Mg	0.00	0.00	0.00	0.00	0.00	0.00	0.00	0.00	0.00	0.00	0.00	0.00	0.00	0.00	0.00	0.00	0.00	0.00	0.00	0.00
M2Fe2	0.05	0.14	0.09	0.15	0.12	0.07	0.10	0.12	0.10	0.10	0.05	0.12	0.11	0.15	0.11	0.02	0.08	0.09	0.10	0.10
M2Mn	0.01	0.01	0.01	0.01	0.01	0.01	0.00	0.01	0.01	0.01	0.01	0.01	0.01	0.01	0.01	0.01	0.00	0.01	0.01	0.01
M2Ca	0.90	0.79	0.86	0.83	0.83	0.89	0.86	0.83	0.79	0.85	0.89	0.78	0.84	0.81	0.83	0.91	0.87	0.85	0.77	0.85
M2Na	0.01	0.01	0.02	0.01	0.02	0.01	0.02	0.02	0.03	0.02	0.01	0.03	0.02	0.03	0.02	0.02	0.02	0.01	0.02	0.02
Sum_cat	4.00	4.00	4.00	4.00	4.00	4.00	4.00	4.00	4.00	4.00	4.00	4.00	4.00	4.00	4.00	4.00	4.00	4.00	4.00	4.00

Table 6.iii Average D1 orthopyroxene values for both core and rim analyses as determined by electron microprobe, with Fe^{3+} calculated from stoichiometry

	Orthopyroxene Cores					Orthopyroxene Rims				
Sample	D1.338	D1.355	D1.380	D1.399	D1.578	D1.338	D1.355	D1.380	D1.399	D1.578
Depth*	-98	-115	-140	-159	-338	-98	-115	-140	-159	-338
SiO_2	54.09	54.79	53.71	52.33	54.94	54.15	54.79	53.82	52.42	55.12
TiO_2	0.12	0.09	0.09	0.07	0.10	0.08	0.13	0.08	0.07	0.09
Al_2O_3	0.80	0.57	0.76	0.78	0.87	0.58	0.63	0.66	0.58	0.73
FeO	17.39	20.04	18.92	24.19	13.94	18.28	20.56	18.68	25.30	14.18
Cr_2O_3	0.14	0.09	0.12	0.15	0.33	0.10	0.13	0.11	0.08	0.24
MnO	0.37	0.47	0.34	0.49	0.28	0.46	0.44	0.37	0.52	0.30
MgO	25.71	23.14	24.99	20.64	28.69	25.61	22.63	25.37	19.99	28.71
CaO	1.28	0.81	1.08	1.20	0.74	0.70	0.83	0.87	0.95	0.53
Na_2O	0.11	0.01	0.05	0.14	0.09	0.03	0.01	0.06	0.12	0.11
Total	100.03	100.02	100.07	100.02	100.01	100.00	100.16	100.05	100.05	100.02
WO	2.52	1.88	2.13	2.45	1.43	1.37	1.70	1.71	1.95	1.02
EN	70.26	65.68	68.32	58.38	77.12	69.93	64.64	69.15	56.86	77.14
FS	27.23	32.86	29.55	39.17	21.45	28.71	33.66	29.14	41.20	21.84
En #	72.07	66.79	69.81	59.84	78.24	70.90	65.76	70.35	57.96	77.94
TSi	1.97	2.03	1.96	1.97	1.96	1.98	2.03	1.96	1.98	1.97
TAl	0.03	0.00	0.03	0.03	0.04	0.03	0.00	0.03	0.02	0.03
TFe3	0.00	0.00	0.00	0.00	0.00	0.00	0.00	0.01	0.00	0.00
M1Al	0.00	0.03	0.00	0.00	0.00	0.00	0.03	0.00	0.01	0.00
M1Ti	0.00	0.00	0.00	0.00	0.00	0.00	0.00	0.00	0.00	0.00
M1Fe3	0.03	0.00	0.03	0.03	0.03	0.02	0.00	0.03	0.02	0.03
M1Fe2	0.00	0.00	0.00	0.00	0.00	0.00	0.00	0.00	0.00	0.00
M1Cr	0.00	0.00	0.00	0.01	0.01	0.00	0.00	0.00	0.00	0.01
M1Mg	0.96	0.97	0.96	0.96	0.96	0.98	0.97	0.96	0.97	0.96
M2Mg	0.43	0.31	0.40	0.20	0.57	0.42	0.29	0.42	0.15	0.57
M2Fe2	0.50	0.62	0.54	0.73	0.39	0.54	0.64	0.53	0.78	0.40
M2Mn	0.01	0.02	0.01	0.02	0.01	0.01	0.01	0.01	0.02	0.01
M2Ca	0.05	0.03	0.04	0.05	0.03	0.03	0.03	0.03	0.04	0.02
M2Na	0.01	0.00	0.00	0.01	0.01	0.00	0.00	0.01	0.01	0.01
Sum_cat	4.00	4.00	4.00	4.00	4.00	4.00	4.00	4.00	4.00	4.00

Table 6.iv Average D1 plagioclase core and rim analyses as determined by electron microprobe

	Plagioclase Cores									Plagioclase Rims								
Sample	D1.259	D1.309	D1.316	D1.338	D1.355	D1.380	D1.399	D1.476	D1.578	D1.259	D1.309	D1.316	D1.338	D1.355	D1.380	D1.399	D1.476	D1.578
Depth*	-19	-89	-76	-98	-115	-140	-159	-236	-338	-19	-89	-76	-98	-115	-140	-159	-236	-338
SiO_2	51.89	52.01	51.31	51.07	50.60	50.15	49.63	49.96	50.41	52.57	52.31	52.46	52.03	52.48	49.93	49.28	50.00	50.60
TiO_2	0.04	0.01	0.02	0.03	0.02	0.01	0.02	0.03	0.02	0.01	0.02	0.03	0.01	0.03	0.02	0.01	0.02	0.00
Al_2O_3	30.67	30.65	31.12	31.25	31.57	31.89	32.19	31.93	31.69	30.28	30.46	30.36	30.58	30.27	32.04	32.46	31.91	31.57
FeO	0.10	0.10	0.11	0.08	0.08	0.14	0.13	0.14	0.10	0.11	0.14	0.12	0.24	0.10	0.18	0.14	0.16	0.13
MnO	0.00	0.02	0.01	0.02	0.01	0.01	0.02	0.01	0.01	0.02	0.02	0.00	0.03	0.01	0.01	0.02	0.02	0.01
MgO	0.01	0.01	0.00	0.01	0.01	0.00	0.00	0.02	0.02	0.01	0.01	0.01	0.05	0.01	0.01	0.00	0.00	0.03
CaO	13.12	13.08	13.61	13.77	14.16	14.55	14.90	14.66	14.32	12.55	12.77	12.69	12.80	12.84	14.69	15.17	14.66	14.19
Na_2O	3.90	3.95	3.64	3.53	3.32	3.11	2.87	3.03	3.23	4.21	4.09	4.16	3.97	4.17	3.01	2.71	3.04	3.32
K_2O	0.23	0.17	0.15	0.23	0.19	0.14	0.20	0.16	0.15	0.19	0.16	0.17	0.24	0.28	0.10	0.16	0.16	0.15
Total	99.96	99.96	99.97	99.99	99.96	99.99	99.96	99.96	99.96	99.96	100.01	99.99	99.93	99.96	99.99	99.96	99.96	100.00
Ab	34.50	35.10	32.30	31.20	29.50	27.70	25.50	27.00	28.70	37.40	36.28	36.87	35.40	36.80	26.90	24.20	27.00	29.50
An	64.10	63.90	66.80	67.40	69.40	71.50	73.30	72.10	70.40	61.50	62.65	62.12	63.20	61.60	72.50	74.70	72.00	69.70
Or	1.30	1.00	0.90	1.40	1.10	0.80	1.20	0.90	0.90	1.10	1.06	1.02	1.40	1.60	0.60	1.10	0.90	0.90
An #	65.01	64.55	67.41	68.36	70.17	72.08	74.19	72.75	71.04	62.18	63.33	62.75	64.10	62.60	72.94	75.53	72.73	70.26
Si	9.43	9.44	9.33	9.29	9.22	9.14	9.06	9.12	9.19	9.53	9.49	9.51	9.45	9.52	9.11	9.01	9.12	9.22
Al	6.56	6.55	6.66	6.70	6.77	6.85	6.92	6.86	6.80	6.47	6.51	6.48	6.54	6.47	6.88	6.99	6.86	6.77
Ti	0.01	0.00	0.00	0.00	0.00	0.00	0.00	0.00	0.00	0.00	0.00	0.00	0.00	0.00	0.00	0.00	0.00	0.00
Fe2	0.02	0.02	0.02	0.01	0.01	0.02	0.02	0.02	0.02	0.02	0.02	0.02	0.04	0.02	0.03	0.02	0.02	0.02
Mn	0.00	0.00	0.00	0.00	0.00	0.00	0.00	0.00	0.00	0.00	0.00	0.00	0.00	0.00	0.00	0.00	0.00	0.00
Mg	0.00	0.00	0.00	0.00	0.00	0.00	0.00	0.01	0.01	0.00	0.00	0.00	0.01	0.00	0.00	0.00	0.00	0.01
Ca	2.55	2.54	2.65	2.69	2.76	2.84	2.92	2.87	2.80	2.44	2.48	2.47	2.49	2.46	2.87	2.97	2.87	2.77
Na	1.38	1.39	1.28	1.25	1.17	1.10	1.02	1.07	1.14	1.48	1.44	1.46	1.40	1.47	1.07	0.96	1.08	1.17
K	0.05	0.04	0.04	0.05	0.04	0.03	0.05	0.04	0.04	0.05	0.04	0.04	0.06	0.06	0.02	0.04	0.04	0.03
Sum_cat	19.99	19.99	19.99	20.00	19.99	19.99	19.99	19.99	19.99	19.99	19.99	19.98	19.99	20.00	19.98	19.99	19.99	19.99

Table 6.v Plagioclase separates as determined by XRF on fusion discs

Plagioclase Separates														
Sample	D1.104	D1.129	D1.184	D1.195	D1.249	D1.259	D1.271	D1.274	D1.276	D1.298	D1.322	D1.332	D1.338	D1.355
Depth*	136	111	58	45	-9	-19	-31	-34	-36	-58	-82	-92	-98	-115
SiO_2	52.88	54.76	53.38	54.89	60.42	58.31	57.08	59.70	60.18	56.17	53.75	59.59	53.45	55.03
TiO_2	0.21	0.27	0.20	0.20	0.17	0.20	0.17	0.17	0.13	0.14	0.18	0.16	0.14	0.14
Al_2O_3	28.98	22.29	28.95	27.50	24.19	23.89	26.23	24.98	25.02	26.15	28.70	25.92	28.38	27.87
FeO	0.59	2.11	0.47	1.69	0.43	1.30	0.53	0.76	0.24	0.24	0.35	0.21	0.29	0.19
Fe_2O_3	0.66	2.35	0.52	1.88	0.48	1.45	0.59	0.84	0.27	0.27	0.39	0.23	0.32	0.21
MnO	0.01	0.01	0.01	0.01	0.02	0.04	0.20	0.01	0.04	0.02	0.01	0.00	0.01	0.00
MgO	0.35	4.80	1.01	0.52	0.50	1.51	0.41	0.90	0.34	0.39	0.41	0.21	0.31	0.21
CaO	12.88	12.38	11.55	10.10	9.37	10.06	11.03	9.93	10.36	12.45	13.15	10.63	13.32	12.64
Na_2O	3.71	3.01	4.22	4.65	3.51	3.85	3.87	3.21	3.07	4.06	3.23	2.58	3.75	3.66
K_2O	0.30	0.10	0.13	0.22	1.35	0.66	0.21	0.25	0.58	0.34	0.12	0.64	0.32	0.24
P_2O_5	0.02	0.03	0.04	0.03	0.01	0.00	0.20	0.02	0.00	0.01	0.05	0.04	0.00	0.01
Total	100.00	100.00	100.01	100.00	100.02	99.99	99.99	99.99	99.99	100.00	99.99	100.00	100.00	100.01
Ab	33.70	30.30	39.50	44.80	36.60	39.10	38.30	36.20	33.50	36.40	30.50	29.10	33.10	33.90
An	64.60	69.00	59.70	53.80	54.10	56.50	60.30	61.90	62.40	61.60	68.70	66.20	65.00	64.70
Or	1.80	0.70	0.80	1.40	9.30	4.40	1.40	1.90	4.10	2.00	0.80	4.70	1.90	1.50
An#	65.72	69.49	60.18	54.56	59.65	59.10	61.16	63.10	65.07	62.86	69.25	69.46	66.28	65.62
Si	9.60	9.99	9.65	9.92	10.77	10.48	10.24	10.61	10.69	10.14	9.72	10.58	9.71	9.93
Al	6.20	4.79	6.16	5.85	5.08	5.06	5.54	5.22	5.24	5.56	6.11	5.42	6.07	5.92
Fe3	0.09	0.32	0.07	0.26	0.06	0.20	0.08	0.11	0.04	0.04	0.05	0.03	0.04	0.03
Ti	0.03	0.04	0.03	0.03	0.02	0.03	0.02	0.02	0.02	0.02	0.02	0.02	0.02	0.02
Mn	0.00	0.00	0.00	0.00	0.00	0.01	0.03	0.00	0.01	0.00	0.00	0.00	0.00	0.00
Mg	0.10	1.31	0.27	0.14	0.13	0.41	0.11	0.24	0.09	0.11	0.11	0.06	0.08	0.06
Ca	2.51	2.42	2.24	1.96	1.79	1.94	2.12	1.89	1.97	2.41	2.55	2.02	2.59	2.44
Na	1.31	1.06	1.48	1.63	1.21	1.34	1.35	1.11	1.06	1.42	1.13	0.89	1.32	1.28
K	0.07	0.02	0.03	0.05	0.31	0.15	0.05	0.06	0.13	0.08	0.03	0.15	0.07	0.06
Sum_cat	19.90	19.95	19.83	19.82	19.38	19.61	19.54	19.28	19.24	19.78	19.73	19.16	19.91	19.73

Table 6.v Continued

Plagioclase Separates													
Sample	D1.374	D1.380	D1.419	D1.424	D1.434	D1.435	D1.436	D1.455	D1.464	D1.468	D1.476	D1.556	D1.578
Depth*	-134	-140	-179	-184	-194	-195	-196	-215	-224	-228	-236	-316	-336
SiO_2	58.56	52.66	52.04	50.98	48.69	52.78	50.47	52.41	51.29	49.67	49.81	48.65	50.59
TiO_2	0.19	0.15	0.15	0.26	0.16	0.14	0.15	0.14	0.14	0.14	0.12	0.19	0.13
Al_2O_3	26.21	29.51	28.59	30.38	32.96	28.75	30.93	28.88	30.18	32.17	31.95	31.82	30.95
FeO	0.08	0.31	0.43	0.83	0.40	0.54	0.49	0.83	0.40	0.28	0.25	0.16	0.32
Fe_2O_3	0.09	0.34	0.48	0.92	0.44	0.60	0.54	0.92	0.44	0.31	0.28	0.18	0.36
MnO	0.00	0.02	0.01	0.00	0.01	0.01	0.01	0.00	0.00	0.01	0.03	0.04	0.04
MgO	0.16	0.34	0.29	0.54	0.34	0.40	0.30	0.93	0.32	0.16	0.30	0.37	0.45
CaO	11.33	13.85	14.95	14.04	14.38	13.45	14.88	13.85	14.58	14.74	15.72	15.56	15.32
Na_2O	3.26	2.95	3.16	2.66	2.94	3.74	2.64	2.96	2.98	2.71	1.88	3.04	1.96
K_2O	0.19	0.17	0.32	0.21	0.06	0.11	0.06	0.10	0.05	0.08	0.11	0.14	0.17
P_2O_5	0.00	0.01	0.00	0.01	0.02	0.02	0.02	0.02	0.02	0.03	0.00	0.00	0.01
Total	99.99	100.00	99.99	100.00	100.00	100.00	100.00	100.01	100.00	100.00	100.00	99.99	100.00
Ab	33.80	27.50	27.20	25.20	26.90	33.20	24.20	28.00	26.90	24.90	16.10	25.90	16.70
An	64.90	71.40	71.00	73.50	72.70	66.10	75.40	71.40	72.80	74.80	83.20	73.30	80.20
Or	1.30	1.00	1.80	1.30	0.40	0.70	0.40	0.60	0.30	0.40	0.70	0.80	1.10
Anit	65.75	72.19	72.30	74.47	72.99	66.57	75.70	71.83	73.02	75.03	83.79	73.89	81.09
Si	10.44	9.55	9.51	9.29	8.89	9.59	9.20	9.52	9.34	9.05	9.08	8.93	9.22
Al	5.50	6.30	6.15	6.52	7.09	6.16	6.64	6.18	6.47	6.91	6.86	6.88	6.64
Fe3	0.01	0.05	0.07	0.13	0.06	0.08	0.07	0.13	0.06	0.04	0.04	0.03	0.05
Ti	0.03	0.02	0.02	0.04	0.02	0.02	0.02	0.02	0.02	0.02	0.02	0.03	0.02
Mn	0.00	0.00	0.00	0.00	0.00	0.00	0.00	0.00	0.00	0.00	0.01	0.01	0.01
Mg	0.04	0.09	0.08	0.15	0.09	0.11	0.08	0.25	0.09	0.04	0.08	0.10	0.12
Ca	2.16	2.69	2.93	2.74	2.81	2.62	2.91	2.66	2.85	2.88	3.07	3.06	2.99
Na	1.13	1.04	1.12	0.94	1.04	1.32	0.93	1.04	1.05	0.96	0.59	1.08	0.70
K	0.04	0.04	0.08	0.05	0.01	0.03	0.01	0.02	0.01	0.01	0.03	0.03	0.04
Sum_cat	19.36	19.78	19.95	19.84	20.02	19.92	19.88	19.82	19.89	19.92	19.76	20.14	19.78

6.1.2: Borehole D2

Samples were taken at intervals of 10m to 36m from a depth of -148m within the MZ to 111m above the MZ/UZ boundary. A total of 177 points were analysed. Average values are available in Figures 6.E to 6.G and summarised in Tables 6.vi - 6.viii. A complete data set is provided in Appendix 4, p liii - lxiii.

6.1.2.1: Clinopyroxene

Mg #

Values for cores and rims are very similar throughout the sampled succession, with an Mg # range of 65 - 75 for cores and 63 - 76 for rims. From the base up to -22m, the magnesium concentration within the cores does not vary outside the values of 72 - 74. The range of values widens within the UZ from 4m, as the Mg # drops to between 65 - 73. Values indicate that the Mg number in the Upper Zone (Figure 6.E) is relatively uniform. Because many of the samples are derived from similarly composed lithological units, lithological control cannot be determined.

Wt % TiO_2

The titanium concentration is greater in the cores for the majority of samples and values are spread over a wider range than for rims. Minimum-maximum values for the core and rim are 0.07 - 0.48 wt % and 0.10 - 0.32 wt %, respectively (Figure 6.E). From the depth of -148m to 14m, values increase with an increase in height in the succession for both cores and rims, from 0.15 - 0.48 and from 0.22 - 0.30, respectively, indicating an upward enrichment. Samples above this, from 14m to 111m, indicate an overall depletion, coinciding with the appearance of magnetite in the lithological succession.

Wt % Al_2O_3

The minimum core value is 0.90 wt % compared with that of 1.14 wt % for the rims. The maximum average is, however, greater than that of the rims with a value of 1.93 wt % compared with 1.80 wt %. Minor fluctuations occur throughout the sequence (Figure 6.E), but overall, the aluminium concentration of the cores is higher. From -148m to 4m above the MZ/UZ boundary, there is a gradual decrease from 1.61 to 1.48 wt % in the cores and from 1.73 to 1.24 wt % in the rims. Between 4m and 14m, a sharp increase in the wt % is noted where values rise by 0.45 to 1.93 for

cores and by 0.48 to 1.72 for rims. Above this, core and rim values indicate a gradual depletion of aluminium to the top of the sampled succession.

Wt % Cr_2O_3

Core values fall between 0 and 0.12 wt %, compared to rim values, which lie between 0.01 - 0.07 wt %. The minimum and maximum values vary erratically throughout the sequence, but the profile shows that there is a relatively constant chromium concentration throughout the Main and Upper Zones (Figure 6.E).

6.1.2.2: Orthopyroxene

En Content

The core and rim values are similar throughout the succession, with minimum and maximums of En_{56} and En_{52}, respectively, and a shared maximum of En_{70}. From -76m to -22m, within the MZ, the En content varies between 65 and 70 and is relatively constant (Figure 6.F). A sharp drop from En_{68} to En_{56} occurs between -22m and 14m within a gabbronorite sequence. This coincides with the first appearance of inverted pigeonite, which replaces primary orthopyroxene. Above 14m, the En content fluctuates between 59 - 61, forming a second relatively constant profile, except for a rim value of En_{51} at the depth of 89m.

Wt % TiO_2

The minimum titanium concentration for the core and rim are 0.09 and 0.06 wt %, respectively, with both attaining maximum values of 0.23 wt %. The overall trend throughout the sequence, from the base of the sampled section at -76m up to 62m above the MZ/UZ boundary, is one of depletion (Figure 6.F). A reversal occurs within the interval from 62m to the uppermost sample at 111m, with an increase from 0.12 to 0.23 for cores. Rim values also increase from 0.06 to 0.23 wt %, with height from 89m to the top.

Wt % Al_2O_3

The aluminium concentration for both cores and rims span 0.63 - 2.16 wt % Al_2O_3. The maximum value, at the top of the sampled sequence, coincides with the greatest titanium at the same depth of

111m, taken from a magnetite-rich leucogabbronorite. The majority of samples, however, fluctuate between a narrower range of values, with a maximum of 1.26 wt % Al_2O_3, which has produced a relatively constant profile from -148m to 89m (Figure 6.F).

Wt % Cr_2O_3

Chromium concentration values are very low, and are probably at the detection limit of the machine. The values range between 0 - 0.04 wt % throughout the sampled sequence for both cores and rims, thus a constant profile has resulted for both the MZ and UZ (Figure 6.F).

6.1.2.3: Plagioclase

An Content

The maximum values for anorthite content for plagioclase cores and rims, found at the depth of -76m, are 75 and 74, respectively. Four samples from -148m up to, and including, -76m gives values that indicate a very gradual increase in An content from 68 to 74. Above, a sample taken from -62m, with a value of 71, marks a downward trend to a depth of 111m, as the plagioclase becomes more sodic. Cores and rims attain values of 50 (Figure 6.G).

Wt % K_2O

The profile shows an increasing potassium concentration from the base to the top of the sampled section for both cores and rims (Figure 6.G). Cores tend to contain larger amounts of potassium than the corresponding rims throughout the succession. They also have a slightly wider range of values, which lie between 0.15 - 0.37 wt % compared to 0.14 - 0.33 wt % for rims.

Wt % FeO

The iron concentration varies little between cores and rims, which have a difference of 0.01 % in their respective minimum and maximum values. The lowest value for both comes from the uppermost sample at 111m, with 0.19 for cores and 0.18 for rims. However, the remaining samples have values which fluctuate between 0.23 and 0.39 wt for cores, and between 0.25 - 0.40 wt % for rims. The FeO concentration shows a relatively constant profile through the Main and Upper Zones (Figure 6.G).

6.1.2.4: D2 Summary

The profiles of the element concentration within clinopyroxene and orthopyroxene grains are reasonably constant in the MZ, but in the UZ there is a decreasing trend which is consistent with normal fractionation. This is true for the enstatite and magnesium concentrations. The phase change from primary orthopyroxene to inverted pigeonite occurs at En_{65}. Orthopyroxenes appear to contain less enstatite than the clinopyroxenes, but the values obtained for the Mg # showed little difference between the two. Although the aluminium concentration is almost similar for clinopyroxenes and orthopyroxenes, and concentrations of the element vary little, within either the cores or rims, the orthopyroxene generally contain lower quantities throughout the sampled section. The same pattern is apparent for chromium concentration, which varies little for either of the pyroxenes up through the succession. Again, the trend is similar for both, but the clinopyroxenes contain slightly higher concentrations of the element, which is also the case for titanium. Initially, the clinopyroxenes show an increase in titanium concentration, but a reversal occurs further up the MZ and continues through the UZ. Within the corresponding clinopyroxene cores, the profile of depletion with height, from the base to the top of the sampled section, mirrors that of the other elements. The downwards trend is attributed to the greater affinity titanium has with magnetite. From the first appearance of magnetite, the quantity of titanium contained within the pyroxenes decreases. Other than this, lithological control is not evident as the samples are from a similar rock type, *i.e.* gabbronorite.

6.1.2.5: Wo-En-Fs Ternary Systems

Data are plotted for the clinopyroxene and orthopyroxene pairs, with isotherms calculated for 0Kbar in Figures 6.H, after Davidson and Lindsley (1989). These indicate the approximate temperatures at which the minerals re-equilibrated. The temperatures range from 600° to 1000° for both pyroxenes at this pressure.

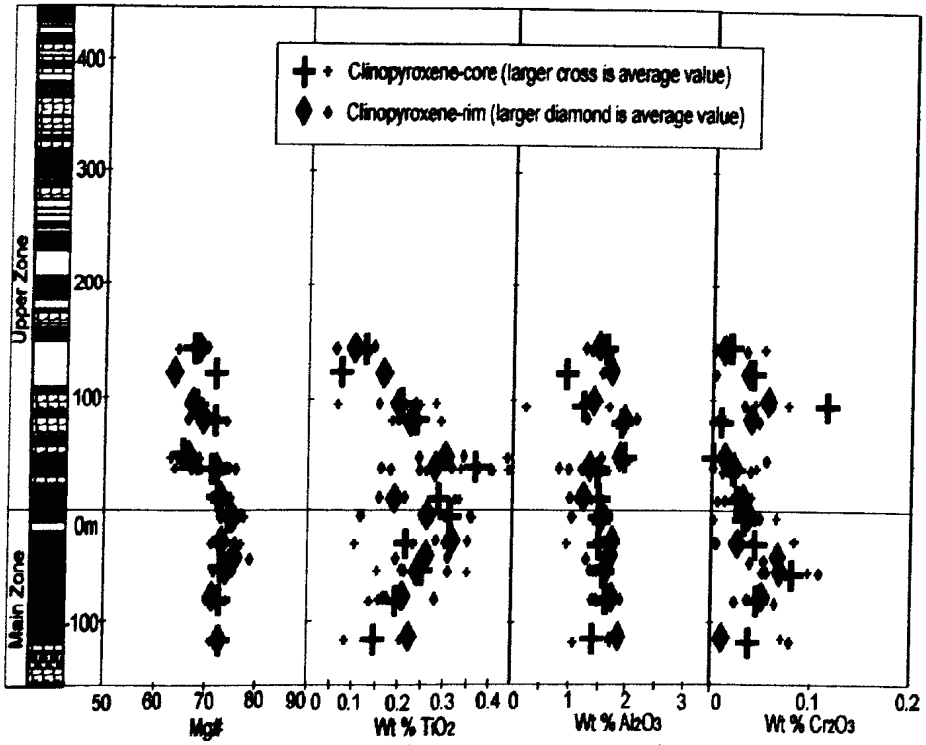

Figure 6.E Electron microprobe analyses of clinopyroxene cores and rims from D2. The Mg content, wt % TiO_2, Al_2O_3 and Cr_2O_3 are plotted against the stratigraphic log and depth relative to the MZ/UZ boundary.

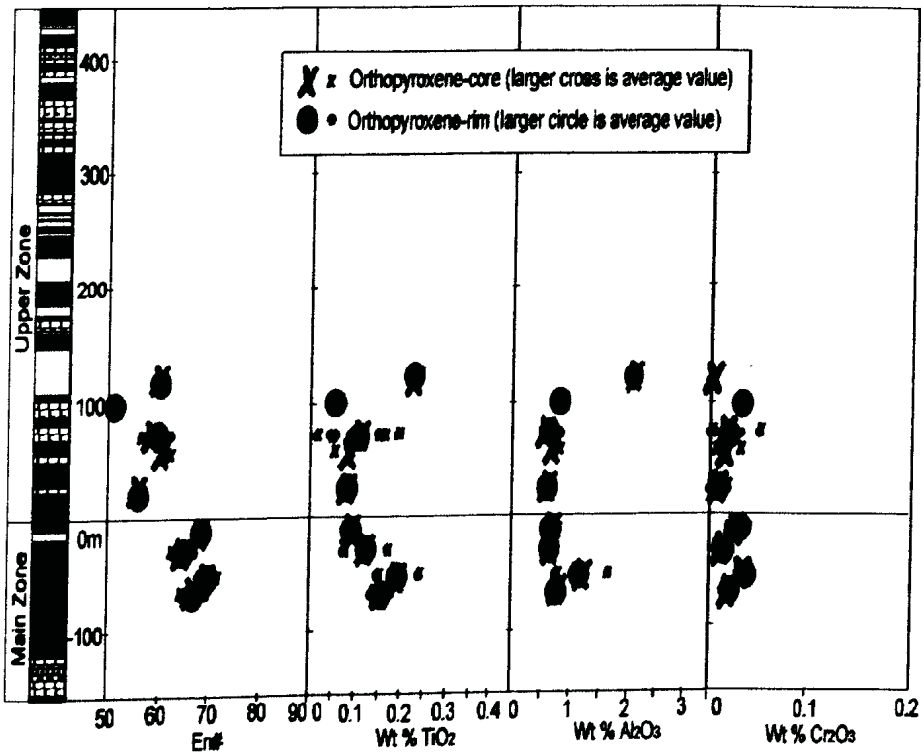

Figure 6.F Electron microprobe analyses of orthopyroxene cores and rims from D2. The En content, wt % TiO_2, Al_2O_3 and Cr_2O_3 are plotted against the stratigraphic log and depth relative to the MZ/UZ boundary.

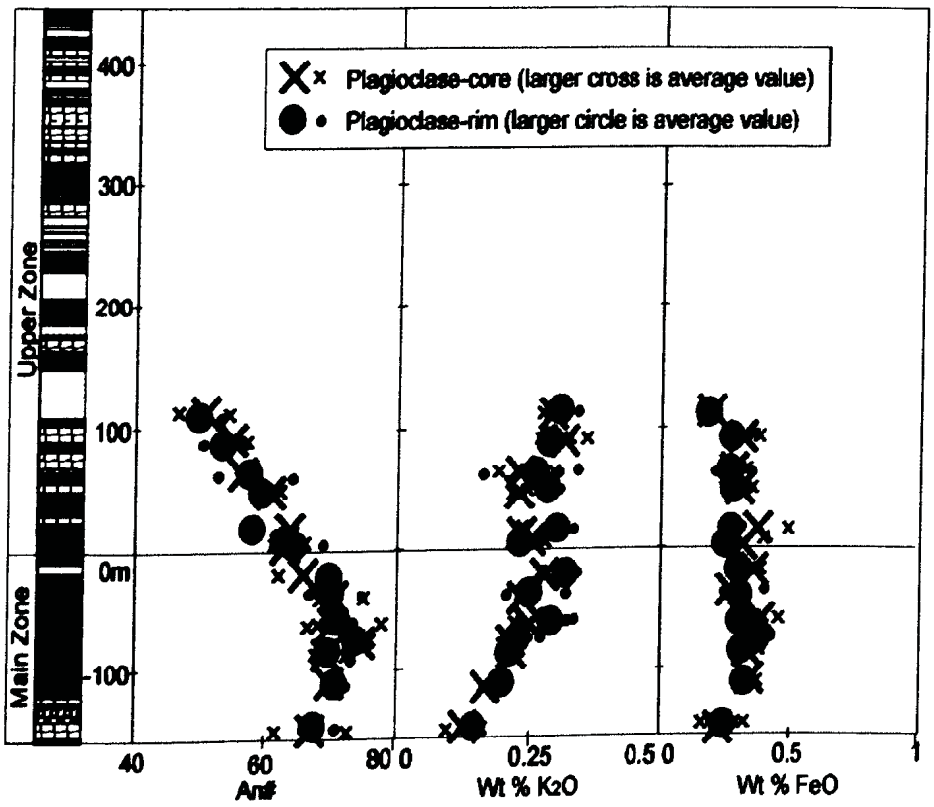

Figure 6.G Electron microprobe analyses of plagioclase cores and rims from D2. The An content, wt % K_2O and FeO are plotted against the stratigraphic log and depth relative to the MZ/UZ boundary.

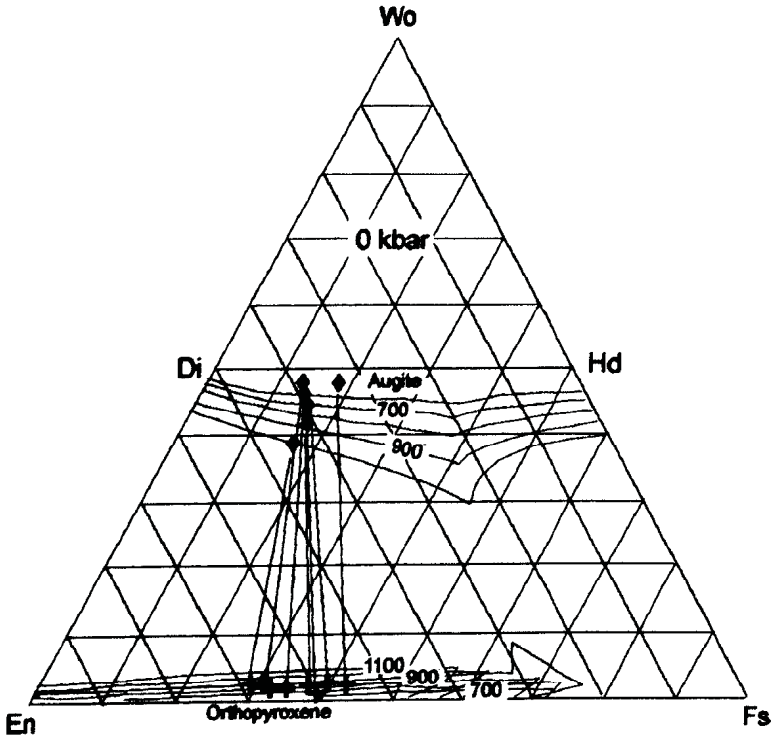

Figure 6.H D2 clinopyroxene and orthopyroxene pairs plotted with isotherms calculated for 0Kbar, after Davidson and Lindsley (1989).

Table 6.vi Electron microprobe analyses for average clinopyroxene cores and rims for borehole D2 with Fe^{3+} calculated from stoichiometry

	Clinopyroxene Cores											
Sample	D2.334	D2.356	D2.383	D2.399	D2.431	D2.441	D2.467	D2.484	D2.507	D2.533	D2.556	D2.593
Depth	111	89	62	46	14	4	-22	-39	-66	-86	-113	-146
SiO_2	53.27	55.32	53.31	53.40	51.42	52.60	53.06	51.96	53.10	53.36	52.94	53.54
TiO_2	0.12	0.07	0.20	0.24	0.46	0.37	0.29	0.31	0.22	0.25	0.19	0.15
Al_2O_3	1.57	0.90	1.20	1.66	1.93	1.46	1.46	1.51	1.49	1.56	1.61	1.40
FeO	11.61	10.07	8.56	9.66	10.73	9.70	9.24	8.16	9.82	9.38	9.15	9.52
Cr_2O_3	0.02	0.04	0.12	0.01	0.00	0.03	0.03	0.04	0.04	0.06	0.04	0.04
MnO	0.29	0.24	0.18	0.32	0.30	0.19	0.25	0.22	0.31	0.25	0.23	0.25
MgO	13.66	14.40	13.70	14.16	11.66	13.16	13.84	13.89	15.61	15.11	13.72	14.26
CaO	18.60	21.76	22.40	20.33	22.92	22.11	21.66	23.66	19.01	19.94	21.89	20.54
Na_2O	0.26	0.11	0.32	0.00	0.56	0.37	0.16	0.27	0.46	0.11	0.31	0.44
Total	100.01	102.94	100.02	100.03	100.05	100.04	100.04	100.04	100.06	100.06	100.12	100.15
WO	39.54	43.66	46.37	42.50	48.00	45.90	44.84	47.79	39.09	41.13	45.31	42.77
EN	40.57	40.19	39.46	41.16	33.96	38.06	39.82	39.00	44.65	43.36	39.53	41.33
FS	19.90	16.16	14.17	16.32	18.04	16.03	15.34	13.21	16.27	15.51	15.16	15.89
Mg #	67.10	71.33	73.57	71.61	65.30	70.38	72.19	74.71	73.29	73.65	72.26	72.23
TSi	2.00	2.01	1.99	2.00	1.93	1.97	1.96	1.93	1.97	1.98	1.97	1.99
TAl	0.01	0.00	0.01	0.01	0.07	0.03	0.02	0.07	0.04	0.02	0.03	0.01
TFe3	0.00	0.00	0.00	0.00	0.00	0.00	0.00	0.00	0.00	0.00	0.00	0.00
M1Al	0.06	0.04	0.04	0.06	0.02	0.03	0.05	0.00	0.03	0.05	0.04	0.05
M1Ti	0.00	0.00	0.01	0.01	0.01	0.01	0.01	0.01	0.01	0.01	0.01	0.00
M1Fe3	0.00	0.00	0.00	0.00	0.06	0.01	0.00	0.07	0.03	0.00	0.00	0.00
M1Fe2	0.16	0.16	0.19	0.13	0.25	0.21	0.16	0.15	0.06	0.10	0.19	0.15
M1Cr	0.00	0.00	0.00	0.00	0.00	0.00	0.00	0.00	0.00	0.00	0.00	0.00
M1Mg	0.78	0.78	0.76	0.79	0.65	0.74	0.77	0.77	0.86	0.84	0.76	0.79
M2Mg	0.00	0.00	0.00	0.00	0.00	0.00	0.00	0.00	0.00	0.00	0.00	0.00
M2Fe2	0.21	0.13	0.06	0.18	0.02	0.06	0.11	0.03	0.20	0.19	0.10	0.14
M2Mn	0.01	0.01	0.01	0.01	0.01	0.01	0.01	0.01	0.01	0.01	0.01	0.01
M2Ca	0.76	0.85	0.89	0.81	0.92	0.89	0.87	0.94	0.75	0.79	0.87	0.82
M2Na	0.02	0.01	0.02	0.00	0.04	0.03	0.01	0.02	0.03	0.01	0.02	0.03
Sum_cat	4.00	4.00	4.00	4.00	4.00	4.00	4.00	4.00	4.00	4.00	4.00	4.00

	Clinopyroxene Rims											
Sample	D2.334	D2.356	D2.383	D2.399	D2.431	D2.441	D2.467	D2.484	D2.507	D2.521	D2.533	D2.556	D2.593
Depth	111	89	62	46	14	4	-22	-39	-62	-76	-86	-113	-146
SiO_2	53.33	54.10	53.26	52.75	52.04	52.72	53.07	52.89	53.54	54.06	53.21	52.97	53.34
TiO_2	0.10	0.16	0.20	0.22	0.30	0.28	0.19	0.26	0.32	0.26	0.24	0.21	0.22
Al_2O_3	1.39	1.57	1.29	1.80	1.72	1.24	1.14	1.45	1.61	1.56	1.51	1.61	1.73
FeO	11.29	13.93	10.83	10.46	10.79	9.39	8.71	8.00	9.31	8.42	8.99	9.43	9.67
Cr_2O_3	0.01	0.03	0.05	0.04	0.01	0.02	0.03	0.03	0.03	0.06	0.07	0.05	0.01
MnO	0.29	0.23	0.20	0.27	0.28	0.21	0.27	0.23	0.30	0.23	0.23	0.27	0.26
MgO	14.14	13.89	12.66	13.55	12.24	13.87	13.84	13.79	14.73	15.00	14.70	13.56	14.90
CaO	19.29	20.10	21.19	20.43	22.44	21.98	22.57	22.84	19.97	19.81	20.78	22.13	19.59
Na_2O	0.27	0.22	0.25	0.44	0.29	0.28	0.36	0.49	0.25	0.57	0.33	0.20	0.34
Total	100.12	104.26	99.96	99.99	100.13	100.01	100.01	100.00	100.06	99.99	100.06	100.44	100.06
WO	40.18	39.82	44.66	42.86	46.63	45.06	46.47	47.14	41.63	41.76	42.91	45.56	40.75
EN	41.00	36.29	37.19	39.57	35.41	39.57	39.06	39.60	42.74	44.00	42.23	38.85	43.13
FS	18.83	21.89	18.15	17.58	17.96	15.37	14.45	13.26	15.63	14.24	14.86	15.59	16.12
Mg #	68.53	63.62	67.20	69.24	66.34	72.03	73.01	74.92	73.22	75.54	73.96	71.36	72.79
TSi	1.99	1.96	2.00	1.97	1.96	1.97	1.96	1.96	1.99	2.00	1.96	1.97	1.96
TAl	0.01	0.04	0.00	0.03	0.04	0.03	0.02	0.04	0.01	0.00	0.03	0.03	0.02
TFe3	0.00	0.00	0.00	0.00	0.00	0.00	0.00	0.00	0.00	0.00	0.00	0.00	0.00
M1Al	0.05	0.02	0.06	0.05	0.03	0.02	0.03	0.03	0.06	0.07	0.04	0.04	0.06
M1Ti	0.00	0.00	0.01	0.01	0.01	0.01	0.01	0.01	0.01	0.01	0.01	0.01	0.01
M1Fe3	0.00	0.03	0.00	0.00	0.02	0.02	0.01	0.03	0.00	0.00	0.00	0.00	0.00
M1Fe2	0.16	0.20	0.22	0.19	0.26	0.18	0.20	0.17	0.11	0.10	0.14	0.20	0.11
M1Cr	0.00	0.00	0.00	0.00	0.00	0.00	0.00	0.00	0.00	0.00	0.00	0.00	0.00
M1Mg	0.79	0.75	0.71	0.76	0.69	0.77	0.76	0.76	0.82	0.83	0.81	0.75	0.83
M2Mg	0.00	0.00	0.00	0.00	0.00	0.00	0.00	0.00	0.00	0.00	0.00	0.00	0.00
M2Fe2	0.20	0.20	0.12	0.14	0.07	0.09	0.06	0.05	0.16	0.17	0.14	0.09	0.19
M2Mn	0.01	0.01	0.01	0.01	0.01	0.01	0.01	0.01	0.01	0.01	0.01	0.01	0.01
M2Ca	0.77	0.78	0.85	0.82	0.90	0.86	0.90	0.91	0.80	0.79	0.83	0.86	0.78
M2Na	0.02	0.02	0.02	0.03	0.02	0.02	0.03	0.04	0.02	0.04	0.02	0.01	0.02
Sum_cat	4.00	4.00	4.00	4.00	4.00	4.00	4.00	4.00	4.00	4.00	4.00	4.00	4.00

Table 6.vii D2 orthopyroxene average core and rim analyses as determined by electron microprobe with Fe^{3+} calculated from stoichiometry.

	Orthopyroxene Core								Orthopyroxene Rim							
Sample	D2.334	D2.383	D2.399	D2.431	D2.467	D2.484	D2.507	D2.521	D2.334	D2.356	D2.383	D2.431	D2.467	D2.484	D2.507	D2.521
Depth	111	62	46	14	-22	-39	-62	-76	111	89	62	14	-22	-39	-62	-76
SiO_2	54.04	52.96	53.09	52.62	54.11	53.69	53.28	54.34	54.04	54.22	52.96	52.62	54.11	53.69	53.28	54.34
TiO_2	0.23	0.12	0.09	0.09	0.10	0.13	0.20	0.16	0.23	0.06	0.12	0.09	0.10	0.13	0.20	0.16
Al_2O_3	2.16	0.63	0.74	0.64	0.73	0.72	1.26	0.84	2.16	0.85	0.63	0.64	0.73	0.72	1.26	0.84
FeO	23.02	24.55	23.45	25.84	19.36	21.43	18.70	19.96	23.02	29.61	24.55	25.84	19.36	21.43	18.70	19.96
Cr_2O_3	0.00	0.02	0.02	0.01	0.03	0.02	0.04	0.02	0.00	0.03	0.02	0.01	0.03	0.02	0.04	0.02
MnO	0.26	0.55	0.56	0.64	0.45	0.49	0.34	0.46	0.26	0.55	0.55	0.64	0.45	0.49	0.34	0.46
MgO	20.06	20.34	21.21	19.23	24.22	22.96	25.01	23.63	20.06	18.09	20.34	19.23	24.22	22.96	25.01	23.63
CaO	0.00	0.66	0.66	0.75	0.94	0.50	0.81	0.62	0.00	0.71	0.66	0.75	0.94	0.50	0.81	0.62
Na_2O	0.64	0.12	0.14	0.18	0.17	0.00	0.36	0.02	0.64	0.36	0.12	0.18	0.17	0.00	0.36	0.02
Total	100.48	99.95	99.96	100.01	100.13	99.97	100.00	100.07	100.48	104.49	99.95	100.01	100.13	99.97	100.00	100.07
WO	0.00	1.35	1.35	1.56	1.88	1.01	1.60	1.26	0.00	1.43	1.35	1.56	1.88	1.01	1.60	1.26
EN	60.57	58.28	60.32	55.53	67.25	64.48	68.96	66.50	60.57	50.94	58.28	55.53	67.25	64.48	68.96	66.50
FS	39.43	40.37	38.34	42.91	30.87	34.51	29.45	32.24	39.43	47.63	40.37	42.91	30.87	34.51	29.45	32.24
En #	60.57	59.08	61.14	56.41	68.54	65.14	70.07	67.35	60.57	51.68	59.08	56.41	68.54	65.14	70.07	67.35
TSi	2.01	2.00	1.99	2.00	1.98	1.99	1.94	2.00	2.01	1.99	2.00	2.00	1.98	1.99	1.94	2.00
TAl	0.00	0.00	0.01	0.00	0.02	0.01	0.05	0.00	0.00	0.01	0.00	0.00	0.02	0.01	0.05	0.00
TFe3	0.00	0.00	0.00	0.00	0.00	0.00	0.00	0.00	0.00	0.00	0.00	0.00	0.00	0.00	0.00	0.00
M1Al	0.10	0.03	0.02	0.03	0.02	0.02	0.00	0.04	0.10	0.03	0.03	0.03	0.02	0.02	0.00	0.04
M1Ti	0.01	0.00	0.00	0.00	0.00	0.00	0.01	0.01	0.01	0.00	0.00	0.00	0.00	0.00	0.01	0.01
M1Fe3	0.00	0.00	0.00	0.00	0.01	0.00	0.07	0.00	0.00	0.00	0.00	0.00	0.01	0.00	0.07	0.00
M1Fe2	0.00	0.00	0.00	0.00	0.00	0.00	0.00	0.00	0.00	0.00	0.00	0.00	0.00	0.00	0.00	0.00
M1Cr	0.00	0.00	0.00	0.00	0.00	0.00	0.00	0.00	0.00	0.00	0.00	0.00	0.00	0.00	0.00	0.00
M1Mg	0.90	0.97	0.96	0.97	0.97	0.97	0.92	0.96	0.90	0.97	0.97	0.97	0.97	0.97	0.92	0.96
M2Mg	0.22	0.17	0.21	0.12	0.35	0.30	0.44	0.34	0.22	0.02	0.17	0.12	0.35	0.30	0.44	0.34
M2Fe2	0.72	0.77	0.74	0.82	0.59	0.67	0.50	0.62	0.72	0.91	0.77	0.82	0.59	0.67	0.50	0.62
M2Mn	0.01	0.02	0.02	0.02	0.01	0.02	0.01	0.01	0.01	0.02	0.02	0.02	0.01	0.02	0.01	0.01
M2Ca	0.00	0.03	0.03	0.03	0.04	0.02	0.03	0.03	0.00	0.03	0.03	0.03	0.04	0.02	0.03	0.03
M2Na	0.05	0.01	0.01	0.01	0.01	0.00	0.03	0.00	0.05	0.03	0.01	0.01	0.01	0.00	0.03	0.00
Sum_cat	4.00	4.00	4.00	4.00	4.00	4.00	4.00	4.00	4.00	4.00	4.00	4.00	4.00	4.00	4.00	4.00

Table 6.viii Average plagioclase core and rim analyses for borehole D2, determined by electron microprobe

	Plagioclase Cores													Plagioclase Rims											
Sample	D2.334	D2.356	D2.383	D2.399	D2.431	D2.441	D2.467	D2.484	D2.507	D2.521	D2.533	D2.558	D2.593	D2.334	D2.356	D2.383	D2.399	D2.431	D2.441	D2.467	D2.484	D2.507	D2.521	D2.533	D2.558	D2.593
Depth*	111	89	62	46	14	4	-22	-39	-62	-76	-86	-113	-148	111	89	62	46	14	4	-22	-39	-62	-76	-86	-113	-148
SiO_2	54.98	55.55	53.22	54.74	53.45	51.83	51.49	51.02	51.77	49.15	50.96	48.89	45.88	54.80	55.73	54.61	54.54	53.30	51.46	52.28	51.90	51.69	49.01	49.46	49.66	46.66
TiO_2	0.01	0.01	0.02	0.01	0.04	0.03	0.02	0.01	0.04	0.03	0.01	0.02	0.02	0.01	0.01	0.02	0.01	0.02	0.03	0.01	0.03	0.01	0.00	0.00	0.01	0.01
Al_2O_3	26.81	28.32	28.72	28.73	28.12	28.94	27.56	28.97	28.72	27.97	27.53	27.41	27.79	27.09	28.45	28.77	28.90	27.89	29.04	27.75	29.42	28.47	28.45	27.70	27.31	28.10
FeO	0.19	0.32	0.28	0.30	0.38	0.32	0.35	0.28	0.39	0.37	0.34	0.35	0.23	0.18	0.31	0.29	0.31	0.29	0.27	0.32	0.33	0.33	0.40	0.34	0.36	0.25
MnO	0.02	0.00	0.03	0.00	0.02	0.01	0.00	0.00	0.00	0.00	0.01	0.01	0.01	0.00	0.03	0.01	0.00	0.00	0.04	0.01	0.01	0.01	0.01	0.03	0.01	0.00
MgO	0.02	0.02	0.00	0.00	0.05	0.00	0.00	0.00	0.05	0.00	0.00	0.00	0.00	0.00	0.01	0.06	0.01	0.02	0.00	0.01	0.00	0.00	0.00	0.02	0.00	0.00
CaO	9.87	11.22	11.73	12.02	12.24	12.84	13.94	14.78	14.90	14.94	14.44	14.71	11.02	9.84	11.27	11.31	11.94	12.12	12.53	13.98	14.89	14.84	15.14	15.23	14.56	11.46
Na_2O	5.34	5.04	4.96	4.23	3.85	4.10	4.00	3.28	3.43	2.72	3.45	3.40	2.96	5.38	5.42	4.57	4.50	4.74	3.78	3.38	3.51	3.36	2.91	3.58	3.36	2.96
K_2O	0.34	0.37	0.28	0.27	0.28	0.30	0.33	0.28	0.29	0.26	0.26	0.19	0.15	0.32	0.30	0.27	0.29	0.31	0.25	0.33	0.27	0.30	0.23	0.22	0.20	0.14
Total	97.57	100.85	99.23	100.30	98.43	98.36	97.89	98.62	99.80	95.45	98.99	94.99	88.05	97.62	101.53	100.11	100.52	98.69	97.39	98.08	100.36	99.00	96.16	96.61	95.46	89.59
Ab	48.50	43.90	42.70	38.30	35.70	36.00	33.60	28.20	28.90	24.40	29.80	29.20	32.30	48.60	45.70	41.60	39.90	40.70	34.80	29.60	29.50	28.60	25.50	29.50	29.10	31.50
An	49.50	54.00	55.80	60.10	62.70	62.30	64.60	70.20	69.40	74.10	68.80	69.70	66.60	49.30	52.60	56.80	58.40	57.50	63.70	68.20	69.10	69.80	73.20	69.30	69.70	67.50
Or	2.00	2.10	1.60	1.60	1.70	1.70	1.80	1.60	1.60	1.50	1.40	1.10	1.10	1.90	1.70	1.60	1.70	1.80	1.50	1.90	1.50	1.70	1.30	1.20	1.20	1.00
An#	50.51	55.16	56.65	61.08	63.72	63.38	65.78	71.34	70.60	75.23	69.78	70.48	67.34	50.25	53.51	57.72	59.41	58.55	64.67	69.59	70.08	70.93	74.16	70.14	70.55	68.18
Si	10.14	9.95	9.73	9.86	9.82	9.58	9.63	9.45	9.51	9.42	9.60	9.44	9.42	10.10	9.93	9.88	9.82	9.80	9.58	9.70	9.45	9.54	9.34	9.41	9.52	9.42
Al	5.82	5.97	6.18	6.09	6.09	6.30	6.07	6.32	6.21	6.32	6.11	6.23	6.72	5.88	5.97	6.11	6.13	6.04	6.37	6.07	6.31	6.19	6.39	6.21	6.17	6.68
Ti	0.00	0.00	0.00	0.00	0.01	0.00	0.00	0.00	0.01	0.01	0.00	0.00	0.00	0.00	0.00	0.00	0.00	0.00	0.01	0.00	0.00	0.00	0.00	0.00	0.00	0.00
Fe2	0.03	0.05	0.04	0.05	0.06	0.05	0.06	0.04	0.06	0.06	0.05	0.06	0.04	0.03	0.05	0.04	0.05	0.05	0.04	0.05	0.05	0.05	0.06	0.05	0.06	0.04
Mn	0.00	0.00	0.00	0.00	0.00	0.00	0.00	0.00	0.00	0.00	0.00	0.00	0.00	0.00	0.00	0.00	0.00	0.00	0.01	0.00	0.00	0.00	0.00	0.01	0.00	0.00
Mg	0.01	0.01	0.00	0.00	0.01	0.00	0.00	0.00	0.02	0.00	0.00	0.00	0.00	0.00	0.00	0.02	0.00	0.01	0.00	0.00	0.00	0.00	0.00	0.01	0.00	0.00
Ca	1.95	2.15	2.30	2.32	2.41	2.54	2.79	2.93	2.93	3.07	2.91	3.04	2.42	1.94	2.15	2.18	2.30	2.39	2.50	2.78	2.91	2.94	3.09	3.10	2.99	2.48
Na	1.91	1.75	1.76	1.48	1.37	1.47	1.45	1.18	1.22	1.01	1.26	1.28	1.18	1.92	1.87	1.60	1.57	1.69	1.37	1.22	1.24	1.20	1.08	1.32	1.25	1.16
K	0.08	0.09	0.07	0.06	0.07	0.07	0.08	0.07	0.07	0.06	0.06	0.05	0.04	0.08	0.07	0.06	0.07	0.07	0.06	0.08	0.06	0.07	0.06	0.05	0.05	0.04
Sum_Cat	19.94	19.97	20.08	19.86	19.84	20.02	20.09	20.00	20.02	19.94	20.00	20.10	19.82	19.95	20.04	19.89	19.93	20.05	19.93	19.90	20.03	19.99	20.02	20.16	20.04	19.82

6.2: Magnetite Separates

6.2.1: Borehole D2

Magnetite was separated for whole rock sample analysis from borehole D2, between 106m and 432m in the Upper Zone, along with samples collected from ground surface material at various locations on the flank of the Phosiri Dome. A coarse fraction, *i.e.* greater than 125μm, was initially crushed in a mill. A hand held magnet was then passed over the sample, to remove the magnetite and associated ilmenite, from other impurities. A second crushing reduced this fraction to less than 75μm before it was made into briquettes for analysis. The wt % TiO_2, wt % V_2O_5 and Cr ppm concentrations were analysed, using the XRF Trace element reduction program at facilities provided by the Geology Department at the University of the Witwatersrand. The full data is presented in Table 6.ix. Table 6.x contains data that were collected from surface samples, and provide a qualitative record of the titanium and vanadium concentrations found in the surface magnetites, which are analogous to those found at the base of the Upper Zone.

Wt % TiO_2

Three samples, taken from 106m, 152m and 177m within magnetite layers above the base of the Upper Zone, indicate an increase in the titanium concentration from 11.11 wt % to 13.81 wt %, upwards through the sequence (Figure 6.I). The samples above 336m reveal an overall decreasing trend from 12.76 to 10.36, with one exception at 428m, where the TiO_2 concentration is 14.84 wt %.

Wt % V_2O_5

A decrease in the vanadium concentration of the magnetite layers is evident from the values for the three lowermost samples (Figure 6.I). Between 106m and 177m, the wt % V_2O_5 decreases from 2.17 to 1.49, where it remains about this value for the remainder of the samples to 432m, with one exception of 1.92 at 428m.

Cr ppm

The majority of the samples contain less than 1300 ppm of chromium. A single sample, from the base of the sampled section and at a height of 106m, contains 3193 ppm. Four samples, at depths of 177m,

373m, 385m and 397m contain either no detectable amount of chromium or a negligible amount. No clear trend can be discerned for the chromium concentration in these magnetite layers (Figure 6.I).

Table 6.ix D2 Borehole magnetite layers samples, where depth (m) is relative to the MZ/UZ boundary

Sample #	EU-30	EU-37	EU-27	EU-33	EU-26	EU-29	EU-31	EU-38	EU-28	EU-35	EU-32
Depth*	432	428	397	385	373	365	347	336	177	152	106
TiO_2	11.34	14.84	10.36	11.01	11.80	11.53	12.76	11.71	13.81	12.87	11.11
V_2O_5	1.55	1.92	1.44	1.50	1.50	1.48	1.48	1.52	1.49	1.93	2.17
Cr	566	801	0	0	9	843	1082	217	27	1285	3193

Table 6.x Ground surface samples taken from the flanks of the Phosiri Dome

Sample #	EU-71	EU-72	EU-73	EU-74	EU-75	EU-76	EU-77	EU-101	EU-102
TiO_2	11.90	12.70	13.20	12.60	11.80	11.30	6.80	12.20	13.80
V_2O_5	1.73	1.63	1.29	1.72	1.62	1.69	0.98	0.92	0.71
Cr	3904	2003	2710	204	19	2182	990	1830	214

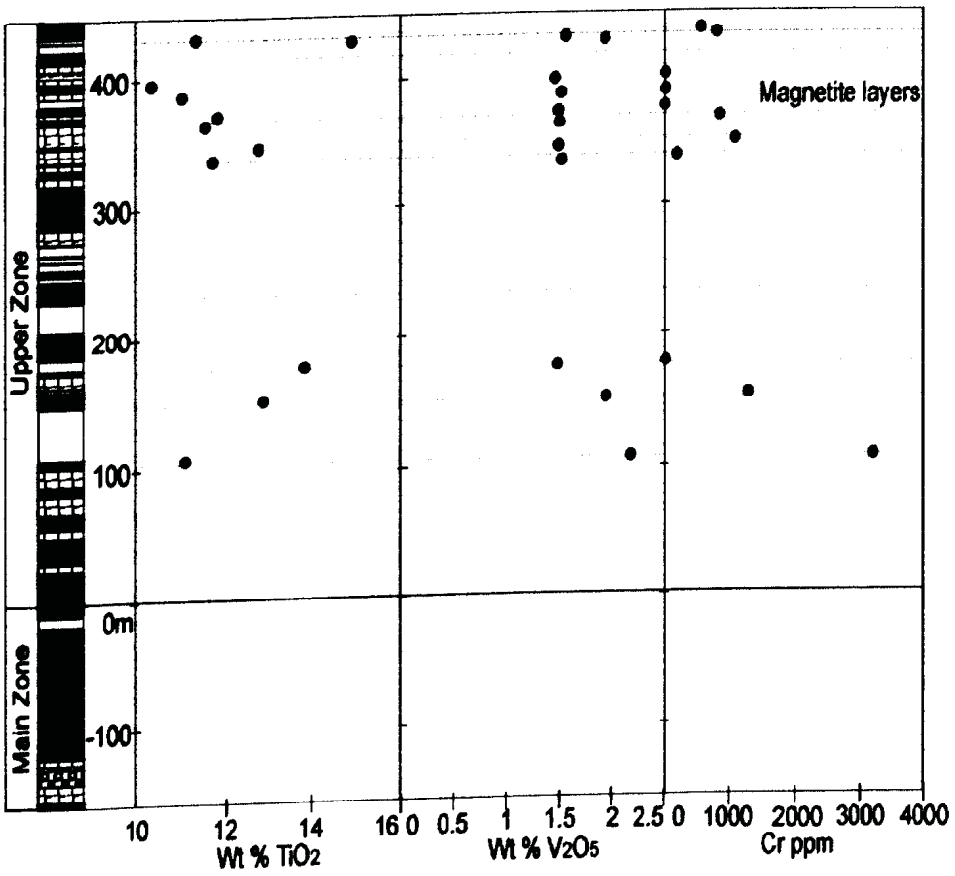

Figure 6.I XRF analyses of magnetite separates from D2. The wt % TiO_2, V_2O_5 and Cr ppm are plotted against the stratigraphic column and depth relative to the MZ/UZ. Magnetite layers are represented as horizontal dashed lines.

6.2.2: Comparisons of Magnetite Layers from the Eastern Limb with Samples taken from the Phosiri Dome.

Magnetite layers of the Upper Zone are categorised by Klemm *et al.* (1985a), according to the vanadium concentration of the individual seams and fall into four groups. The first and lowermost group contain a V_2O_5 concentration of 2.0 - 2.3 wt % and is represented by the first three layers above the base of the Upper Zone, Lower Layers 1 - 3. The second group includes the Main Magnetite Layer (MML) and seven individual layers (Magnetite Layers 1-7), situated above the MML, with vanadium concentrations of 1.5 - 1.86. A third group of magnetite, numbered 8 - 14, contain 0.6 - 0.8 wt % vanadium. The fourth and final group of magnetite layers, 15 - 21, have 0.2 - 0.3 wt % V_2O_5 concentration. Overall, there is a decreasing vanadium concentration upwards through the succession (Groeneveld, 1970; Molyneux, 1970).

Molyneux (1970) notes that below each of the magnetite layers, there is a substantial amount of anorthosite, forming footwalls. The contact between the magnetite layers and their respective footwalls are normally sharp, but the upper contact with their hangingwalls are typically graded (Molyneux, 1970). In D2, however, some of the magnetite layers have sharp contacts with the lithologies that form both the footwall and the hangingwall, for example at 166.16m and 412.50m. Throughout the typical Upper Zone, the magnetite concentration is greater than 5%, and commonly associated with lithologies that contain more clinopyroxene than orthopyroxene (Groeneveld, 1970).

The ternary diagram plotted in Figure 6.J shows both magnetite samples taken from the borecore and the surface. The coloured areas on the graph are the subzone divisions as used by Klemm *et al.* (1985a). Therefore, Subzones A and B correspond to Subzone A in the classification by SACS (1980), which is used in this study. Arrows within the shaded areas denote the differentiation trends, and therefore the cyclicity between the groups of magnetite layers (Klemm *et al.*, 1985a). They maintain that the cyclicity represents the periodic collapse of the cooled and partially crystallised roof rocks, into the convecting magma below and their subsequent entrainment. Klemm *et al.* (1985a) also interpret the lower vanadium concentration in the magnetite layers of the Upper Zone to be indicative of higher fO_2 conditions within the magma during crystallisation, based on the observations of Irving (1978).

When the vanadium concentration of the magnetite samples is compared with the typical values, the samples located at the height of 106m and 152m, correspond with the magnetite layers that are located stratigraphically below the Main Magnetite Layer. The MML is therefore assessed to be between 152m and 177m from the borehole log of D2. The remaining samples all correspond with the magnetite layers found within Subzone A, above the MML, although the Magnetite Layers 1 - 7 are not fully represented within this profile.

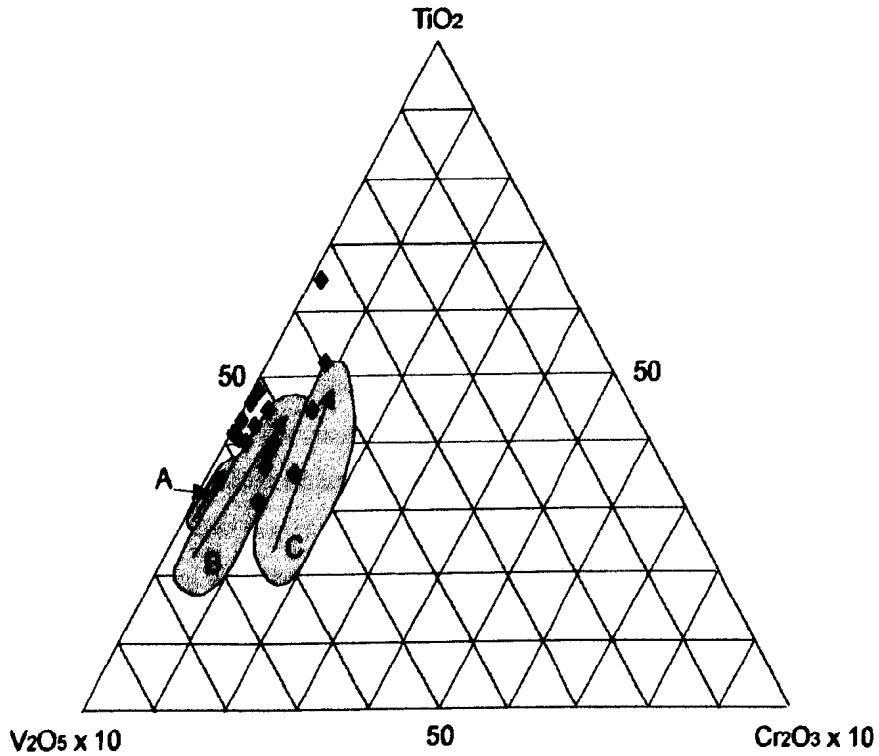

Figure 6.J TiO_2 - V_2O_5 - Cr_2O_3 ternary plot of magnetites within D2 and on surface, with solid blue symbols representing the magnetite layers within D2. The subzones here are A, B and C, as referred to by Klemm *et al.* (1985).

6.3: Comparison of Mineral Analyses and the Typical Sequence of the Eastern Bushveld Complex

Mitchell (1990), using electron microprobe data, derived values for the En and An contents, from the top of the Bastard Reef to the top of the MZ, which confirmed the optically-derived values of Von Gruenewaldt (1973) and Molyneux (1974). These data have been plotted against each other in Figure 6.K, and illustrate the typical sequence of the Complex. A normal fractionation trend is indicated for the MZ. However, Mitchell (1990) highlighted some exceptions: sharp breaks occur at the top of the Main Mottled Anorthosite (MMA), where the En number increases from En_{50} to En_{71}; and at the top of the Upper Mottled Anorthosite (UMA), where there is a change from intercumulus to cumulus pyroxene. The corresponding An of the plagioclase for this lower interval, Subzone A, remains relatively constant between average values of An_{65-71} (Von Gruenewaldt, 1973; Molyneux, 1974; Mitchell, 1990).

Research by Mitchell (1990) and Cawthorn *et al.* (1991) found that Subzone B is represented by a normal fractionation trend up to the level of the Pyroxenite Marker. The En number of the pyroxenes varies between 59 - 65 and the An number of the plagioclase is 59 - 61. The Pyroxenite Marker is represented by a sharp break in the geochemical parameters, where the En number of the pyroxene increases sharply from 60 - 71 and the plagioclase An increases from 60 - 74 (Mitchell, 1990). Cawthorn *et al.* (1991) also describe a normal fractionation trend to 188m below the Pyroxenite Marker within which An number decreases from 67 to 58. A sharp jump to An_{74} is found directly above this marker, coinciding with the other comparative data. The En number of the pyroxenes also indicates a normal differentiation trend, with a reversal occurring above the marker.

Boreholes D1 and D2 reveal similar trends with respect to each other but, when compared to the typical sequence, it would appear that D2 lies stratigraphically above D1. Combining the data from the two produces an incomplete sequence of the typical Main and Upper Zones of the typical Bushveld Complex. This interpretation is supported by the presence of more obvious layers such as the Merensky Reef and the Giant Mottled Anorthosite in borehole D1, which are missing from borehole D2. As samples above the boundary between the Main and Upper Zones in D1 were not analysed by the electron microprobe, direct correlations for the Upper Zone could not be made here.

Based on the analysis of the petrographic evidence presented in Section 5.1, a review of the mineralogy therefore implies that the D1 Main Zone is likely to be represented solely by Subzone A whereas the D2 Main Zone belongs entirely to Subzone C alone. Further confirmation of Subzone A's sole presence in D1 is shown by a decrease in the Cr_2O_3 in both clinopyroxene and orthopyroxene in the western Bushveld Complex at a similar stratigraphic height (Mitchell, 1990). Neither D1 nor D2 show any breaks in the geochemical profiles that are symptomatic of the magma influx at the

Pyroxenite Marker, as described by Von Gruenewaldt (1973), Molyneux (1974), Mitchell (1990) and Cawthorn *et al.* (1991). Moreover, the boreholes do not correlate with the petrographic observations for this portion of the Main Zone, *i.e.* the mineral phase change from inverted pigeonite to orthopyroxene.

The shaded boxes shown in Figure 6.K are the areas on the expected profile, outlined by Von Gruenewaldt (1973), Molyneux (1974) and Mitchell (1990), that most closely correlate with the D1 and D2 trends, as portrayed in Figures 6.A to 6.C and 6.E to 6.G. The width of each of the four shaded areas is defined by the minimum and maximum values of borecore data from the cumulus pyroxenes and plagioclase in D1 and D2. The height of each area is determined by the point of overlap of D1 and D2 with the data from the more typical sequence.

For D1, the En number and Mg number, determined for the orthopyroxene and clinopyroxene, respectively, and the An number, from plagioclase analyses, display a similar trend when compared with Subzone A of the Main Zone. It is noted, however, that the height of the shaded area extends upwards into Subzone B, which conflicts with the evidence determined by petrographic observations. If Subzone B were present in D1, inverted pigeonite would be expected to occur within the sequence (Von Gruenewaldt, 1973; Molyneux, 1974). This clearly is not the case, indicating that either the samples in D1 come from some other portion of the Main Zone, *i.e.* Subzone C or, that the change to inverted pigeonite may have occurred at a different En number. Inversion of pigeonite might not occur if there was a higher water number in the magma, which would reduce the temperature of crystallisation (Cawthorn, 1999 *pers. comm.*)

The Pyroxenite Marker is characterised by geochemical breaks in the sequence between Subzones B and C (see Chapter 2). It is presumed, as shown in Figure 6.L, that Subzone B is absent from both boreholes D1 and D2. As a consequence of this, Subzone C is resting directly above Subzone A. In eliminating the data collated for Subzone B from Von Gruenewaldt (1973), Molyneux (1974) and Mitchell (1990), there is no noticeable geochemical reversal in the An content and a continuation in the apparent differentiation trend is seen across the boundary between the juxtaposed subzones. Similarly, there appears to be a continuation in the apparent differentiation trend for the En content, although the spread of data at the base of Subzone C is great. However, it is believed that only the upper half of Subzone C is present, and the removal of the lower portion would result in a normal differentiation profile, particularly in the data from Molyneux (1974).

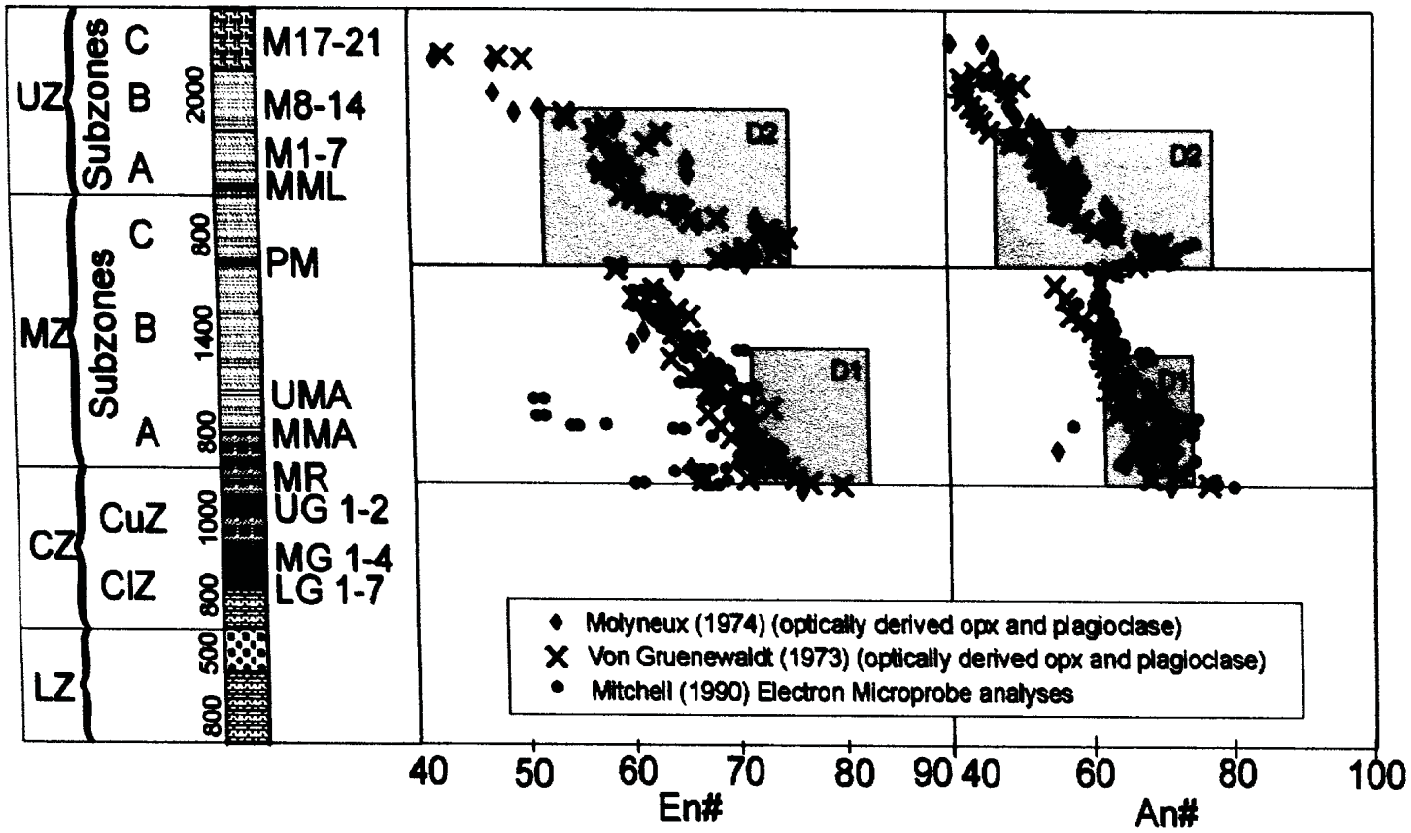

Figure 6.K Comparative data for the eastern and western Bushveld Complex. Dimensions of the shaded areas are defined by the maximum and minimum values from the core analyses of cumulus pyroxenes and plagioclase determined in D1 and D2. Thicknesses of each shaded area are delimited by the points of intersection with the data of Von Gruenewaldt (1973), Molyneux (1974) and Mitchell (1986). The positions of the Merensky Reef (MR) and Pyroxenite Marker (PM) are indicated.

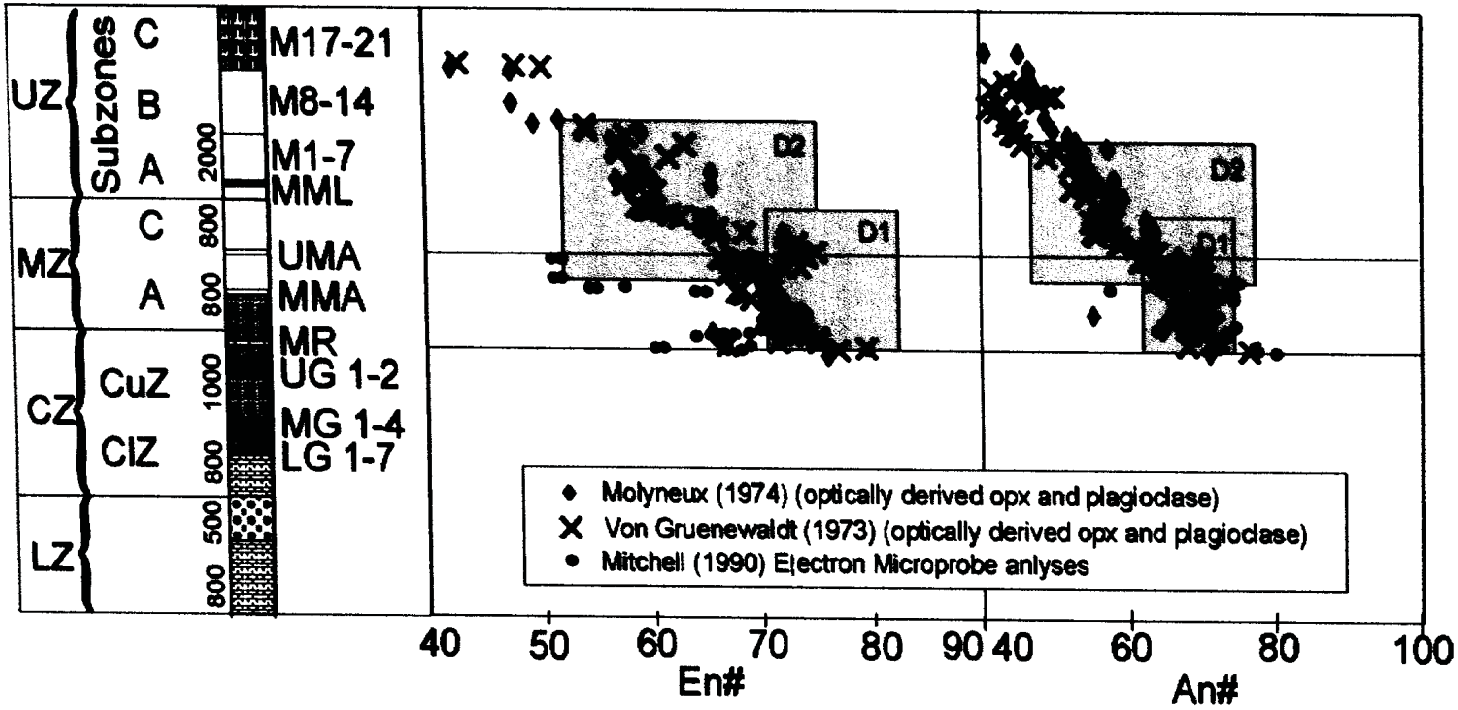

Figure 6.L Comparative data, as for Figure 6.K, with Subzone B of the Main Zone removed so that Subzone C directly overlies Subzone A.

7: WHOLE ROCK XRF GEOCHEMISTRY

The data described in this section were acquired by XRF spectrometry, at the Geology Department at the University of the Witwatersrand, for both D1 and D2 boreholes. BHP Minerals performed additional (XRF) analyses for borehole D2, which are also included in this section. Standard deviations for all elements commonly analysed by XRF normally lie in the range from 0.01 - 0.73 wt % and the average % error is between 0.4 - 11.2. A full description of each of the standards used for the calibration of the PW 1400 XRFS, and the standard deviations for elements are found in Appendix 5. The Cross, Iddings, Pirsson and Washington (CIPW) norm was computed within the MinPet software program, which recalculates the ferric and ferrous iron concentrations, according to the method of Irvine and Barager (1971). Not all samples analysed in this section have corresponding thin sections.

7.1: Borehole D1

Sixty-nine samples, extracted from the borecore, at intervals of up to 10m apart, were analysed. They derive from lithologies between the depths of -379m to -19m in the Main and Critical Zones of the Bushveld mafic sequence. Figures 7.A, 7.B and 7.C show the Mg # [Mg/(Mg+Fe)*100], wt % TiO_2, wt % Al_2O_3, Sr and Zr ppm and wt % K_2O average values and the interelement ratios Cr/Co, Co/V, Cr/V and Sr/Al_2O_3. A representative selection of the XRF analysis is presented in Table 7.i at the end of this section. A full set of data is included within Appendix 6, p lxvi - lxx.

Mg #

The samples range between Mg # 56 and Mg # 81. From the base of the sampled section, the first five samples encountered are from a single feldspathic pyroxenite within the ClZ and, to a depth of -353m within this unit, the Mg # retains a relatively constant value about 80, as shown in Figure 7.A. At -349m, the Mg # drops to 74, but directly above values return to between Mg # 77 - 80 and do not significantly vary up to a depth of -274m.

Where the leucocratic units occur above -269m upwards, the Mg # dips slightly from 70 to 68. This is repeated at -236m, but within a mottled anorthosite. Otherwise the Mg # remains relatively constant around Mg # 79 until -228m. From -227m up to -197m, samples from a single layer of mottled anorthosite provides a wide range of values between Mg # 56 - 70. The higher values are found closer to the base of the layer, while the lowest value occurs at the top. Norites with Mg # values between 70 - 74, at the depth of -195m to -190m, separate this anorthosite from the Giant Mottled Anorthosite